

Supporting Information

Assembling Dense Grid with Green Polyhydroxyurethane and High-capacity Si-based Anode for Lithium Ion Batteries

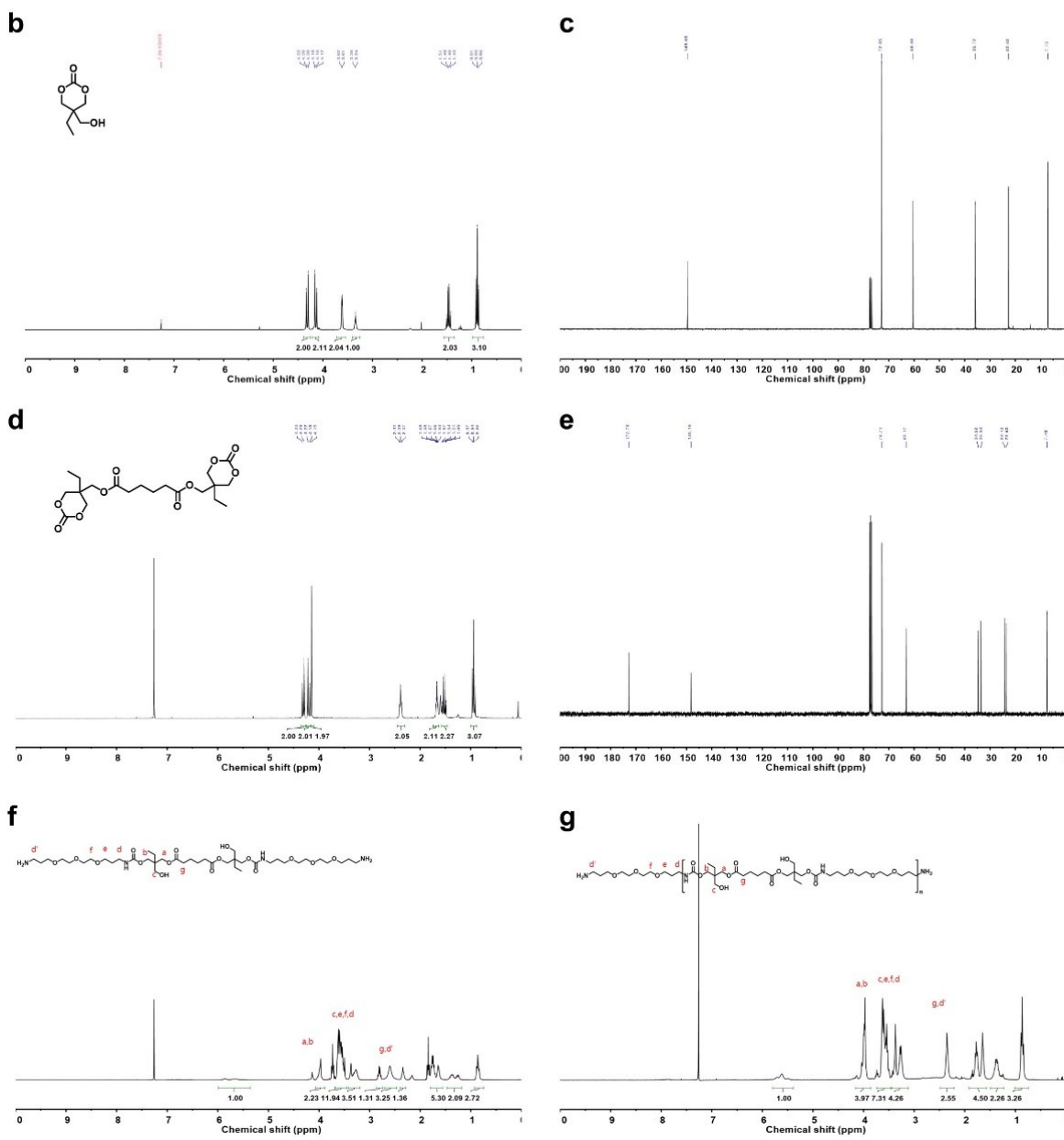
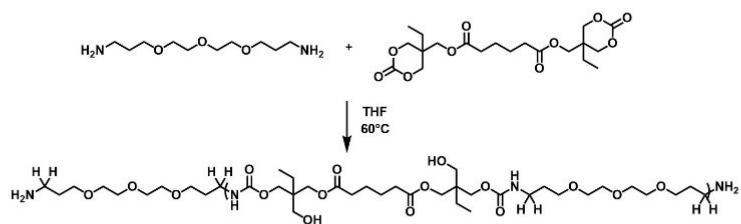
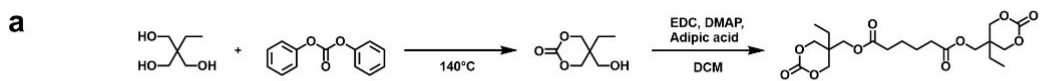


Fig S1. Synthesis of NIPU and NIOU. (a) Synthesis mechanism of NIPU by free-isocyanate route (b) ^1H NMR and (c) ^{13}C NMR spectra (in CDCl_3) of the 5-ethyl-5-(hydroxymethyl)-1,3-dioxan-2-one (d) ^1H NMR and (e) ^{13}C NMR spectra (in CDCl_3) of the Bis((5-ethyl-2-oxo-1,3-dioxan-5-yl)methyl) adipate (f) ^1H NMR spectra (in CDCl_3) of the NIOU (g) ^1H NMR spectra (in CDCl_3) of the NIPU

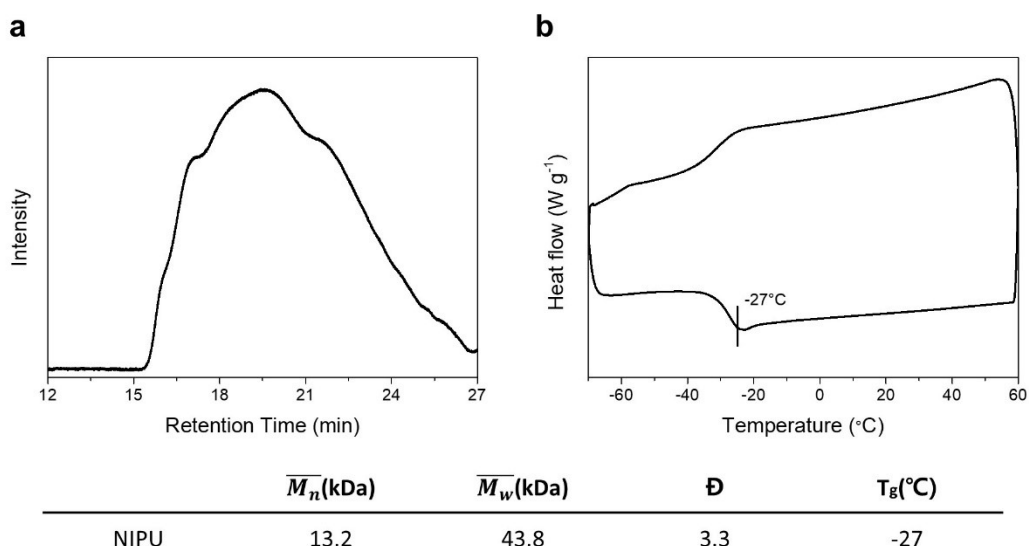


Fig S2. Basic properties of NIPU. (a) GPC spectra (DMF, 1.0 mL min^{-1} ; the molecular weight was calculated with PEO standard) of NIPU (b) DSC curve (N_2 , 50 mL min^{-1} , heating rate: $10 \text{ }^{\circ}\text{C min}^{-1}$, second cycle, exothermic up) of NIPU.

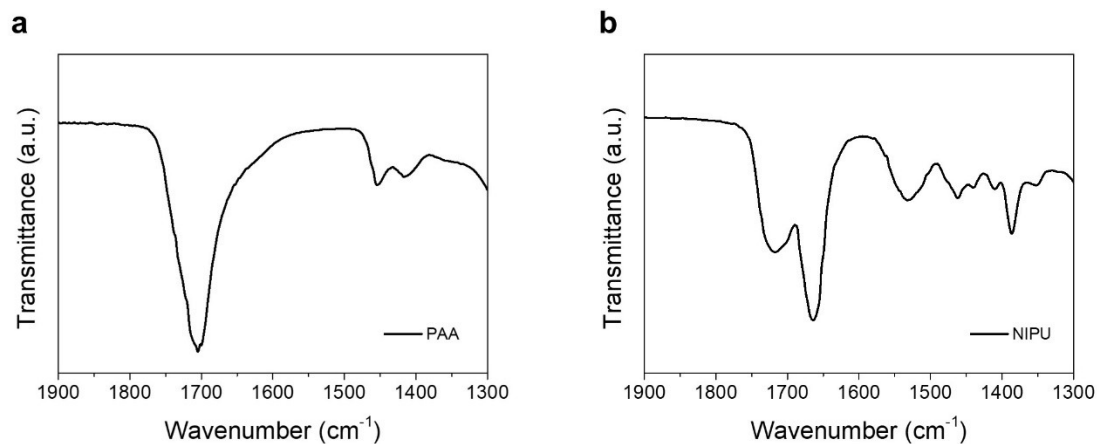


Figure S3. FT-IR spectra of (a) PAA film and (b) NIPU film before curing.

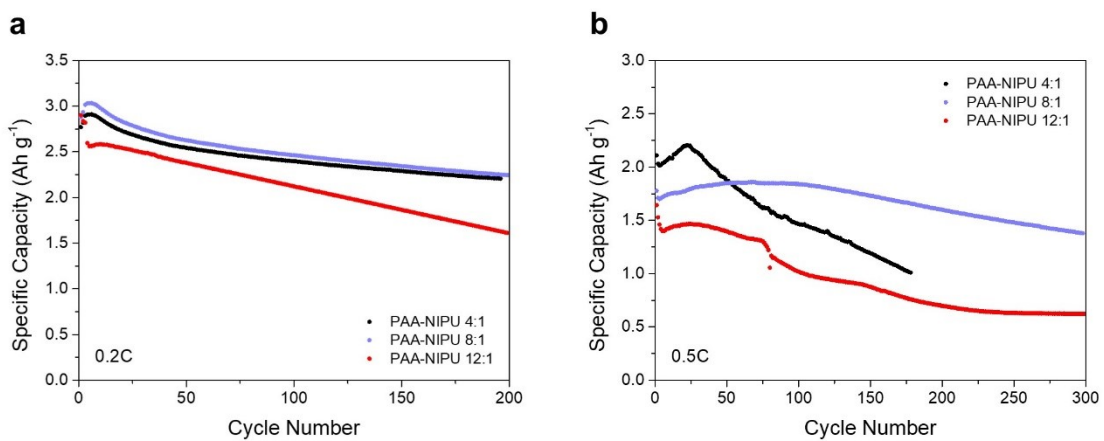


Fig S4. Cycling performances of SiNP electrode fabricated with mixing various ratios between PAA and NIPU. Discharge capacities of SiNP half cell using various mixing ratios of PAA-NIPU binders at (a) 0.2 C and (b) 0.5 C (1 C = 3 A g⁻¹)

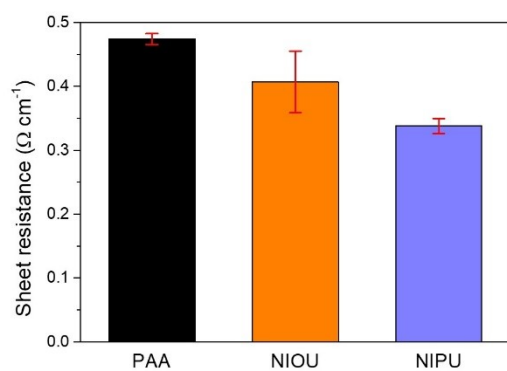


Fig S5. Electrical conductivity comparison. Sheet resistance comparison between SiNP electrodes fabricated with PAA, PAA-NIOU, and PAA-NIPU.

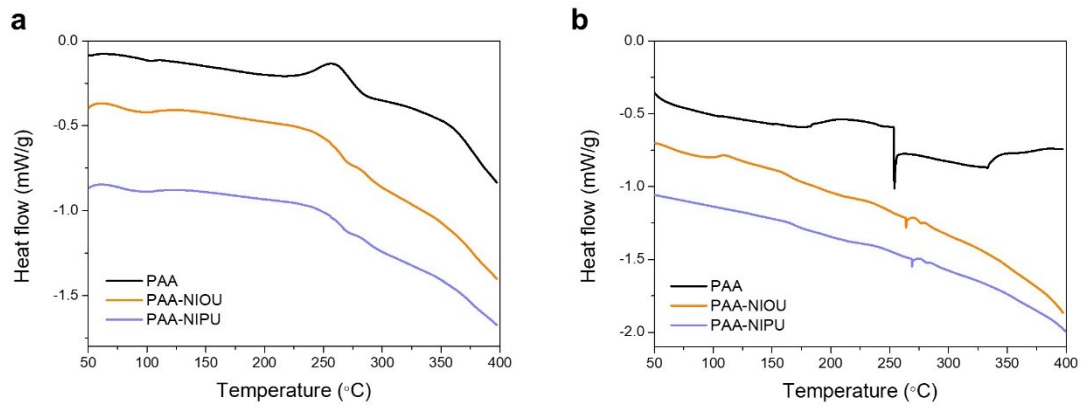


Fig S6. Thermal stability of SiNP electrode. DSC thermograms of SiNP electrode with PAA, PAA-NIOU, and PAA-NIPU binder in (a) fully discharged state and (b) fully charged state.

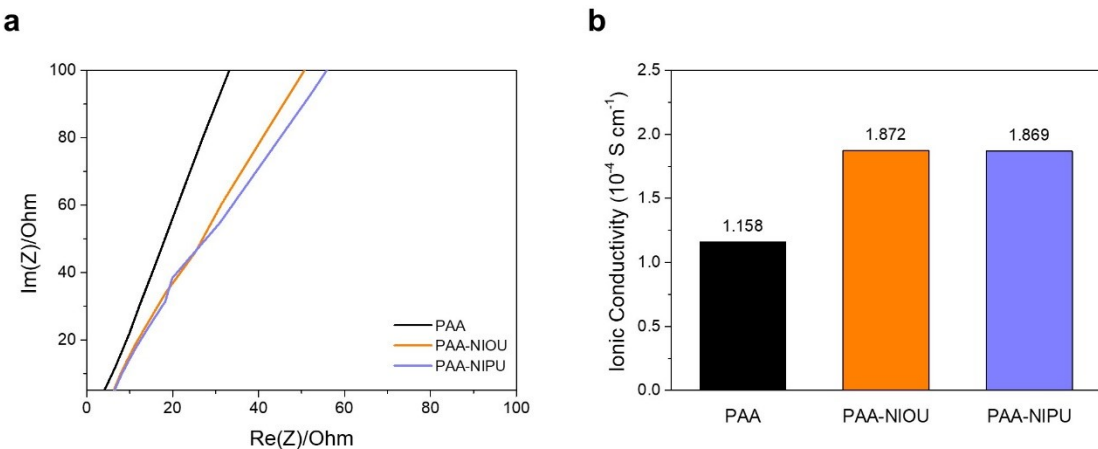


Fig S7. Ion conductivity of polymer film. (a) Nyquist plots of PAA, PAA-NIOU, and PAA-NIPU polymer films. (b) Ionic conductivity of PAA, PAA-NIOU, and PAA-NIPU polymer film.

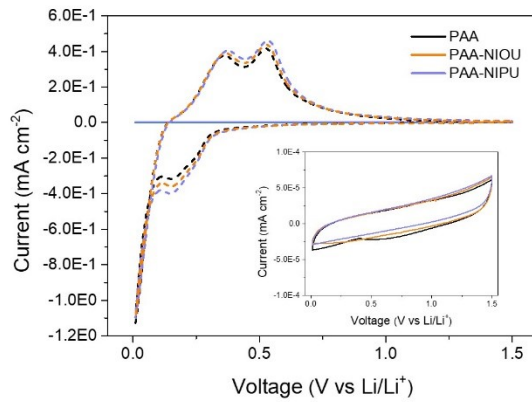


Fig S8. Electrochemical stability of NIPU polymer. Cyclic voltammogram of PAA, PAA-NIOU, and PAA-NIPU electrodes (Solid line: PAA, PAA-NIOU, and PAA-NIPU polymer binder film, Dotted line: PAA, PAA-NIOU, and PAA-NIPU electrode with SiNP) (Inset: Magnification of cyclic voltammetry of PAA, PAA-NIOU, and PAA-NIPU binder film).

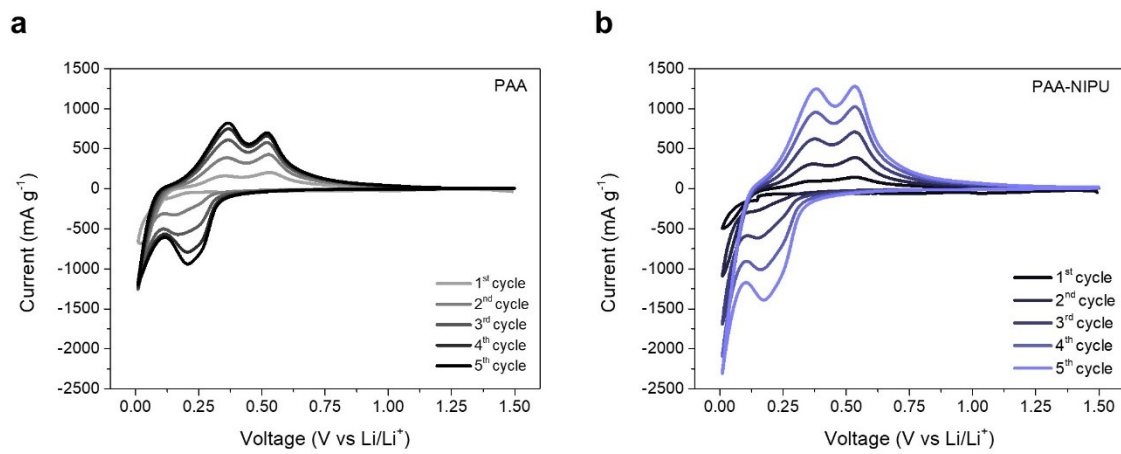


Fig S9. CV analysis with increased cycle number. Cyclic voltammetry curves of PAA and PAA-NIPU electrodes with different cycle numbers.

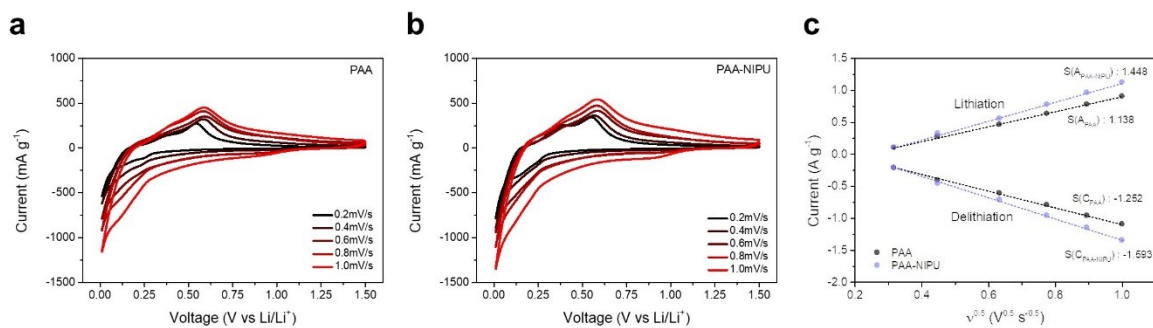


Fig S10. Diffusion coefficient calculation by CV analysis with increased scan rates. Cyclic voltammetry curves of (a) PAA, (b) PAA-NIPU electrodes with different scan rates, and (c) ion diffusion coefficient analysis.

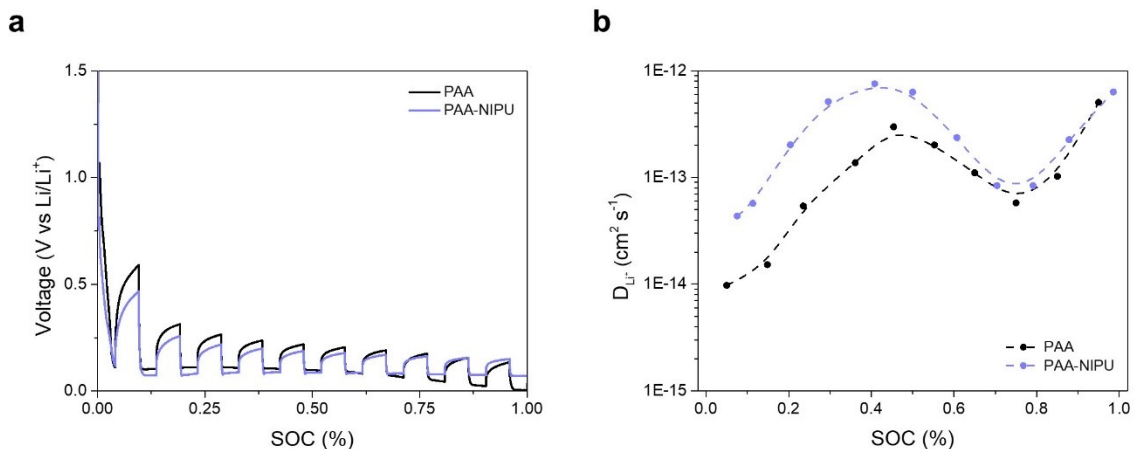


Fig S11. Diffusion coefficient calculation by GITT analysis. (a) GITT measurement results of PAA and PAA-NIPU electrodes. (b) Variation in Li-diffusion coefficient of PAA and PAA-NIPU electrodes depends on the state of charge (SOC) measured by GITT.

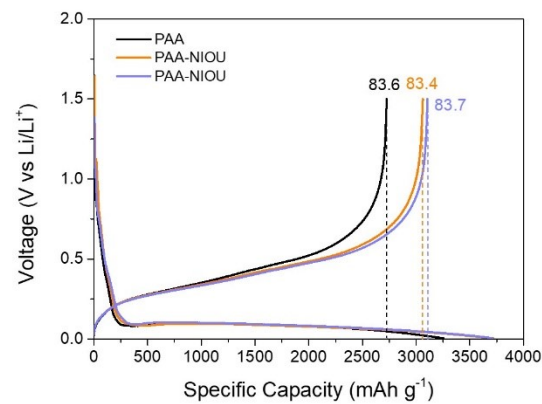


Fig S12. Pre-cycle profiles of SiNP electrode. Initial galvanostatic charge-discharge curves of the SiNP half-cell using PAA, PAA-NIOU, and PAA-NIPU binders at 0.05 C (1 C=3 A g⁻¹).

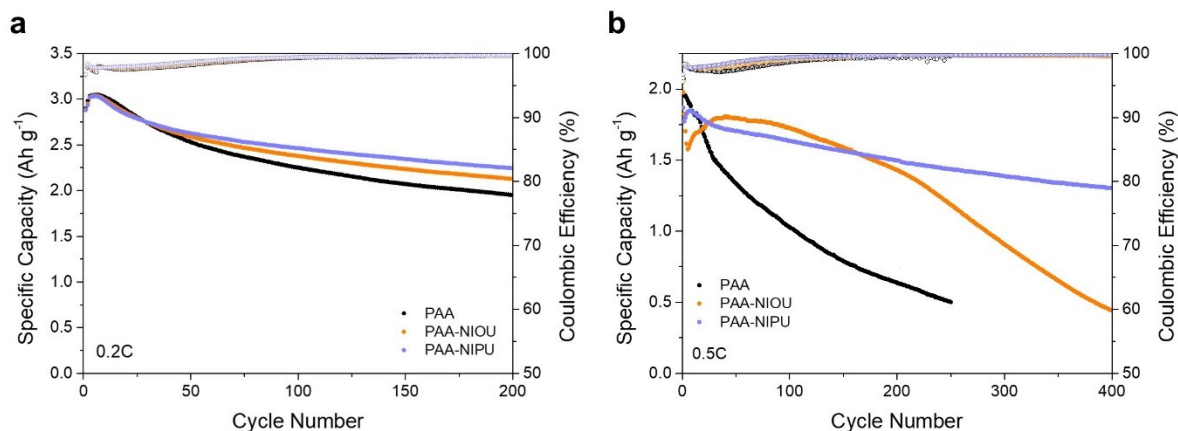


Fig S13. Long-term cycling performances of SiNP electrode at various C-rate. Discharge capacities and corresponding CE of SiNP half cell using PAA, PAA-NIOU, and PAA-NIPU binders at (a) 0.2 C and (b) 0.5 C (1 C=3 A g⁻¹)

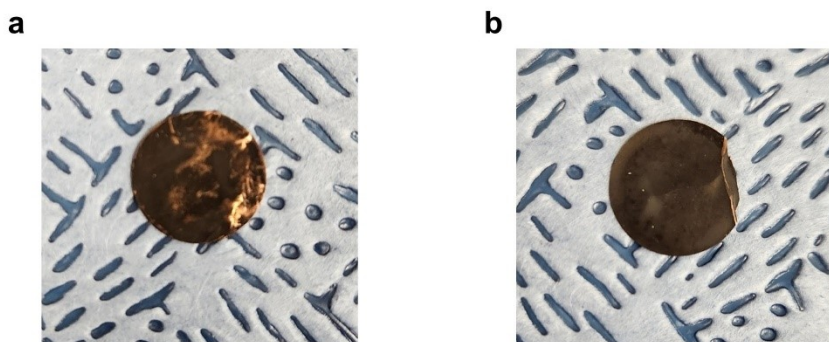


Fig S14. SiNP electrode stability after cycling. Photographs of SiNP electrodes after 200 cycles at 0.5 C (1 C=3 A g⁻¹) using (a) PAA binder and (b) PAA-NIPU electrodes.

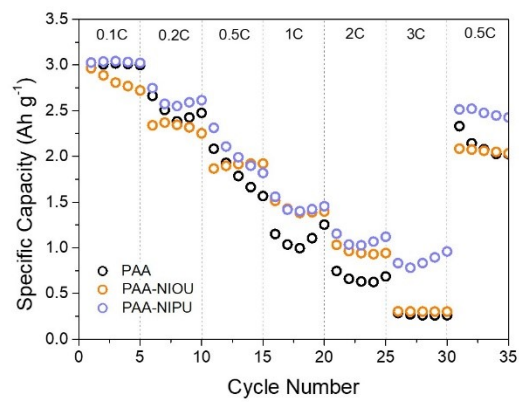


Fig S15. Rate capability of SiNP electrode. Rate capability of the SiNP half cell using PAA, PAA-NIOU, and PAA-NIPU binders at various C-rate (1 C=3 A g⁻¹)

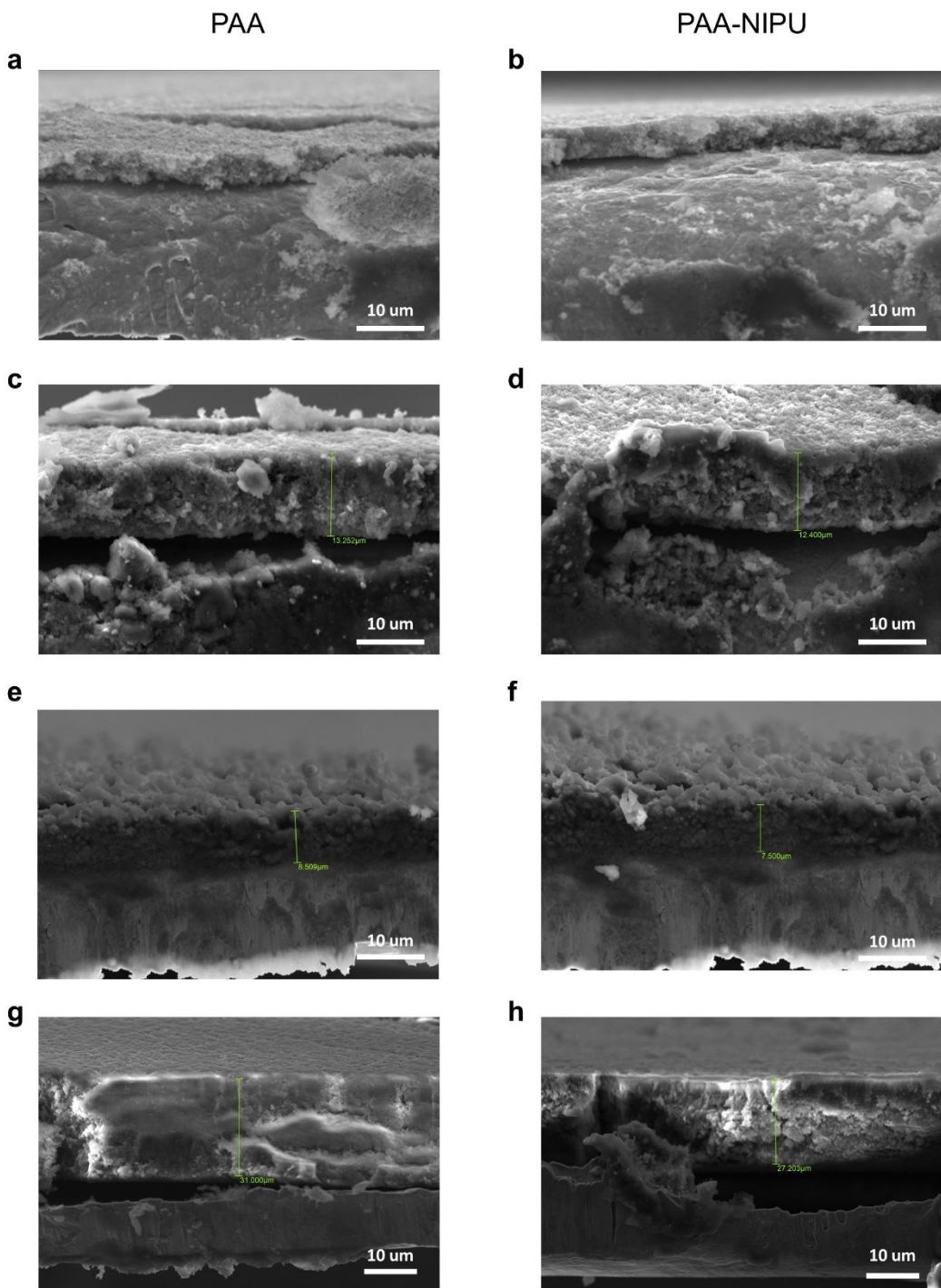


Fig S16. Thickness change of SiNP Electrode after cycling. Cross-sectional SEM images of the SiNP electrodes before cycling, after 1st charge, after 1st discharge, and after the 50th cycle using (a, c, e, g) PAA binder and (b, d, f, h) PAA-NIPU binder, respectively.

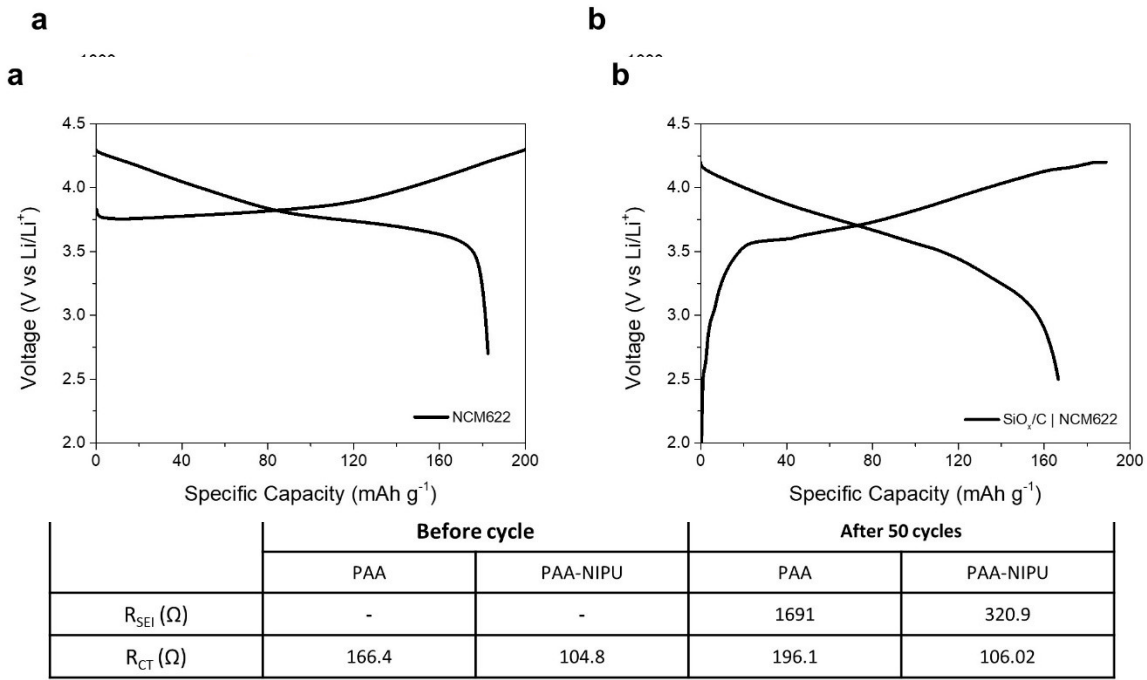


Fig S17. EIS analysis of SiNP electrode. Nyquist plots of the SiNP half-cells using PAA and PAA-NIPU binders (a) before the cycle and (b) after 50 cycles and table of calculated resistances.

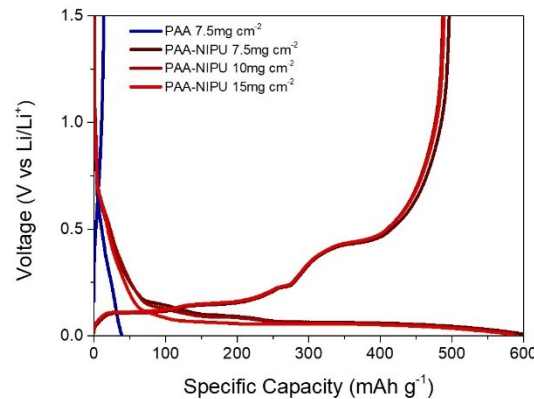


Fig S18. Pre-cycle profiles of SiO_x/C electrode. Initial galvanostatic charge-discharge curves of SiO_x/C half-cell using PAA and PAA-NIPU binders at 0.05 C (1 C=0.5 A g⁻¹).

Fig S19. Pre-cycle profiles of the full-cell. Initial galvanostatic charge-discharge curves of the (a) NCM622 half-cell and (b) $\text{SiO}_x/\text{C}|\text{NCM622}$ full-cell at 0.1 C (1 C = 0.2 A g^{-1}).

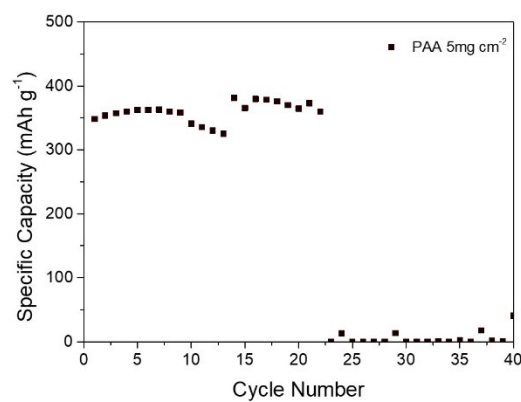


Fig S20. Long-term cycling performance of SiO_x/C electrode. Discharge capacities of the SiO_x/C half-cell using PAA binder at 0.2 C (1 C=0.5 A g^{-1}).

Table S1. Performance comparison of Si-based anode using various binder

Ref.	Binder	Half-Cell			Full Cell	
		Electrode Composition	Active Material Mass Loading (mg/cm ²)	Cycle Retention Current Density	Configuration	Cycle Retention Current Rate
This work	PAA-NIPU	60 : 20 : 20 ^a 80 : 10 : 10 ^b	0.5 15	79.7%@300th (3A/g) 92.5%@50th (0.25A/g)	SiO _x /C NCM622 3.66	85.3%@400th (1C)
18	PAA-PUU	60 : 20 : 20 ^a	0.36 0.78	61%@270th (1.5A/g) 65%200th (1.5A/g)	-	-
21	PAA-BFPU	70 : 20 : 10 ^a	0.95 1.54	88%@200th (2A/g) 86%100th (0.8A/g)	-	-
22	PAA-M-BFPU	80 : 10 : 10 ^a	- 1.2	75.6%@200th (4.2A/g) 69.1%@100th (1.4A/g)	Si NCM811 -	97%@100th (0.5C)
23	PAA-PVA	60 : 20 : 20 ^a	1.5 2.4	61%@250th (4.2A/g) 94%@50th (-)	-	-
S1	PEI-PVA	60 : 20 : 20 ^a	1.8	41.3%@300th (1A/g)	-	-
S2	PAA-SN	60 : 20 : 20 ^a	0.8	72%@500th (-)	-	-
S3	PAA-TA	70 : 20 : 10 ^c	-	73.3%@250th (0.5A/g)	SiO _x NCM811 1.89	87.4%@100th (0.5C)
S4	PDA-PAA-PEO	60 : 20 : 20 ^a	0.4	74%@200th (1.5A/g)	-	-
S5	N-P-LiPN	80 : 10 : 10 ^a	0.94	71%@100th (2.1A/g)	-	-
S6	PEI-PVA	60 : 20 : 20 ^a	1.8~2.7	60.1%@300th (1A/g)	-	-
S7	PFA-PVA	60 : 20 : 20 ^a	0.6	73.6%@300th (0.3A/g)	-	-
S8	PAA-EVA	70 : 20 : 10 ^a	0.6	85%100th (1A/g)	-	-
S9	PAA-SMAS	63:15:22 ^a	0.7	54%@200th (0.5A/g)	-	-

^aSiNP : Binder : Conductive additive / ^bSiO_x/C : Binder : Conductive additive / ^cSiO_x: Binder : Conductive additive

Supporting References

- S1. Z. Liu, S. J. Han, C. Xu, Y. W. Luo, N. Peng, C. Y. Qin, M. J. Zhou, W. Q. Wang, L. W. Chen and S. Okada, *RSC Adv.*, 2016, **6**, 68371-68378.
- S2. T. T. Su, W. F. Ren, J. M. Yuan, K. Wang, B. Y. Chi and R. C. Sun, *J. Ind. Eng. Chem.*, 2022, **109**, 521-529.
- S3. W. T. Tang, L. Feng, X. J. Wei, G. Y. Lai, H. P. Chen, Z. H. Li, X. H. Huang, S. X. Wu and Z. Lin, *ACS Appl. Mater. Interfaces*, 2022, **14**, 56910-56918.
- S4. L. Lü, H. M. Lou, Y. L. Xiao, G. Z. Zhang, C. Y. Wang and Y. H. Deng, *RSC Adv.*, 2018, **8**, 4604-4609.
- S5. Z. H. Li, Y. P. Zhang, T. F. Liu, X. H. Gao, S. Y. Li, M. Ling, C. D. Liang, J. C. Zheng and Z. Lin, *Adv. Energy Mater.*, 2020, **10**.
- S6. T. F. Liu, Q. L. Chu, C. Yan, S. Q. Zhang, Z. Lin and J. Lu, *Adv. Energy Mater.*, 2019, **9**.
- S7. R. N. Guo, S. L. Zhang, H. J. Ying, W. T. Yang, J. L. Wang and W. Q. Han, *ACS Appl. Mater. Interfaces*, 2019, **11**, 14051-14058.
- S8. D. F. Wei, X. X. Yu, Y. W. Luo, X. Gao and S. N. Ma, *Energ Fuels*, 2022, **36**, 4557-4563.